NeuroImage: Clinical 15 (2017) 35–44

Contents lists available at ScienceDirect

NeuroImage: Clinical

journal homepage: www.elsevier.com/locate/ynicl

Identification of brain regions predicting epileptogenesis by serial [^{18}F]GE-180 positron emission tomography imaging of neuroinflammation in a rat model of temporal lobe epilepsy

Vera Russmann[a], Matthias Brendel[b], Erik Mille[b], Angela Helm-Vicidomini[a], Roswitha Beck[b,c], Lisa Günther[b,c], Simon Lindner[b], Axel Rominger[b], Michael Keck[a], Josephine D. Salvamoser[a], Nathalie L. Albert[b], Peter Bartenstein[b], Heidrun Potschka[a,*]

[a] Institute of Pharmacology, Toxicology & Pharmacy, Ludwig-Maximilians-University (LMU), Munich, Germany
[b] Department of Nuclear Medicine, University Hospital Munich, Ludwig-Maximilians-University (LMU), Munich, Germany
[c] German Center for Vertigo and Balance Disorders, DSGZ, Ludwig-Maximilians-University (LMU), Munich, Germany

ARTICLE INFO

Keywords:
Positron emission tomography
Temporal lobe epilepsy
[^{18}F]GE-180
TSPO
Neuroinflammation
Predictive cluster VOI

ABSTRACT

Excessive activation of inflammatory signaling pathways seems to be a hallmark of epileptogenesis. Positron emission tomography (PET) allows in vivo detection of brain inflammation with spatial information and opportunities for longitudinal follow-up scanning protocols.

Here, we assessed whether molecular imaging of the 18 kDa translocator protein (TSPO) can serve as a biomarker for the development of epilepsy. Therefore, brain uptake of [^{18}F]GE-180, a highly selective radioligand of TSPO, was investigated in a longitudinal PET study in a chronic rat model of temporal lobe epilepsy. Analyses revealed that the influence of the epileptogenic insult on [^{18}F]GE-180 brain uptake was most pronounced in the earlier phase of epileptogenesis. Differences were evident in various brain regions during earlier phases of epileptogenesis with [^{18}F]GE-180 standardized uptake value enhanced by 2.1 to 2.7fold. In contrast, brain regions exhibiting differences seemed to be more restricted with less pronounced increases of tracer uptake by 1.8–2.5fold four weeks following status epilepticus and by 1.5–1.8fold in the chronic phase. Based on correlation analysis, we were able to identify regions with a predictive value showing a correlation with seizure development. These regions include the amygdala as well as a cluster of brain areas. This cluster comprises parts of different brain regions, e.g. the hippocampus, parietal cortex, thalamus, and somatosensory cortex.

In conclusion, the data provide evidence that [^{18}F]GE-180 PET brain imaging can serve as a biomarker of epileptogenesis. The identification of brain regions with predictive value might facilitate the development of preventive concepts as well as the early assessment of the interventional success. Future studies are necessary to further confirm the predictivity of the approach.

1. Introduction

The latency period between an epileptogenic brain insult and the development of epilepsy with spontaneous recurrent seizures opens a window of opportunity for preventive concepts. However, translational development and clinical assessment of anti-epileptogenic strategies will only become practicable based on the availability of reliable biomarkers of epileptogenesis (Pitkanen et al., 2013; Pitkanen and Engel, 2014). Indicators of the epileptogenic process are urgently required for stratification of patient subgroups at risk of developing epilepsy following a brain insult (Schmidt, 2012; Pitkanen et al., 2013; Trinka and Brigo, 2014). Considering the duration of the latency period following an epileptogenic insult (Weiss et al., 1986; Trinka and Brigo, 2014; Rao and Parko, 2015), respective biomarkers will additionally be needed for an early assessment of the interventional success (Schmidt, 2012; Pitkanen et al., 2013; Trinka and Brigo, 2014).

Persistent and excessive activation of glia cells resulting in enhanced activation of inflammatory signaling pathways seems to be a hallmark of the process of epileptogenesis following different types of epileptogenic brain damage (Vezzani et al., 2013). Genetic and pharmacological targeting of key inflammatory events confirmed a relevant functional role of inflammation during epileptogenesis

* Corresponding author at: Institute of Pharmacology, Toxicology, and Pharmacy, Ludwig-Maximilians-University, Koeninginstr. 16, D-80539 Munich, Germany.
E-mail address: potschka@pharmtox.vetmed.uni-muenchen.de (H. Potschka).

http://dx.doi.org/10.1016/j.nicl.2017.04.003
Received 6 February 2017; Received in revised form 3 April 2017; Accepted 4 April 2017
Available online 05 April 2017

(Vezzani et al., 2013). Consequently, strong efforts are currently made to develop and assess anti-inflammatory preventive approaches (Ravizza et al., 2011; Vezzani, 2015). The majority of these strategies aim to directly or indirectly interfere with glial activation or its downstream consequences.

Biomarkers compatible with these interventional approaches should provide information about the extent of glia activation and inflammatory responses (Vezzani and Friedman, 2011; Amhaoul et al., 2014). Molecular imaging approaches based on positron emission tomography (PET) allow non-invasive detection of brain inflammation with regional information and opportunities for longitudinal follow-up scanning protocols. PET imaging of neuroinflammation has traditionally used radiotracers binding to the 18 kDa translocator protein (TSPO), which is expressed in the outer membrane of mitochondria from microglia, astrocytes, and macrophages (Ching et al., 2012; Venneti et al., 2013; Gershen et al., 2015). It has been repeatedly described that TSPO imaging provides information about the extent of microglia activation in various disease states (James et al., 2015; Politis et al., 2015; Zurcher et al., 2015).

In a previous study, we have assessed the uptake of the TSPO ligand (*R*)-[^{11}C]PK11195 in the chronic phase of a post-status epilepticus model of mesial temporal lobe epilepsy with spontaneous recurrent seizures (Bogdanovic et al., 2014). Whereas analysis in rats with drug-resistant epilepsy revealed enhanced brain uptake of the tracer in different brain regions, respective data from rats with drug-sensitive epilepsy proved to be in the same range as in electrode-implanted control animals. Thus, we suggested (*R*)-[^{11}C]PK11195 as a biomarker of drug resistance (Bogdanovic et al., 2014). It has previously been stated that PK11195 is characterized by a relatively low brain uptake, and low TSPO affinity. Therefore efforts have been made to develop optimized radiotracers with a highly selective TSPO binding potential. Among these novel TSPO ligands [^{18}F]GE-180 exhibited superiority in terms of brain uptake, affinity and specific binding in an established neuroinflammation model (Wadsworth et al., 2012).

Experimental efforts have already been made to assess alterations in TSPO imaging in the phase following an epileptogenic status epilepticus and during the course of epileptogenesis (Dedeurwaerdere et al., 2012; Amhaoul et al., 2015; Brackhan et al., 2016; Yankam Njiwa et al., 2016). In these studies the radiotracers [^{11}C]PK11195 and [^{18}F]PBR111 have been applied in different chemical post-status epilepticus models and the temporal and spatial patterns of tracer uptake and binding have been evaluated. Following seizure manifestation Amhaoul et al. (2015) have reported a correlation between tracer uptake and seizure frequency.

However, so far none of the studies has combined a longitudinal analysis with repeated scans with subsequent seizure monitoring, so that conclusions about the predictive value are not yet possible based on available data.

Here, we took the TSPO imaging approach one important step further testing the correlation of TSPO imaging data at different stages of epileptogenesis with subsequent seizure development. Therefore, we have selected [^{18}F]GE-180 for a longitudinal PET study in a rat model of epileptogenesis triggered by an electrically-induced status epilepticus. The main aim was to determine whether TSPO imaging with the novel radiotracer can serve as a biomarker for the development of epilepsy. Repeated PET scans were performed at two time points during the latency phase of epileptogenesis and in the early phase following onset of epilepsy with recurrent seizures. A 2-week continuous video/EEG monitoring of spontaneous seizures allowed assessment of a putative correlation between imaging data and the epileptogenic process.

2. Methods

2.1. Preparation of [^{18}F]GE-180

Automated production of [^{18}F]GE-180 (specific activity 1407 ± 484 GBq/μmol) was performed on a FASTlab™ synthesizer with single-use disposable cassettes as previously described (Wickstrom et al., 2014). The pre-filled precursor vial was assembled on the cassette and the cassette was mounted on the synthesizer according to the set-up instructions. The FASTlab™ control software prompts were followed to run the cassette test and to start the synthesis. No carrier added [^{18}F] fluoride was produced via ^{18}O(p, n)^{18}F reaction by proton irradiation of ^{18}O-enriched water and delivered to the ^{18}F incoming reservoir. The fully automated manufacturing process consists of the following steps: trapping of [^{18}F]fluoride on a QMA cartridge; elution using Kryptofix®222, potassium hydrogen carbonate, water and acetonitrile; azeotropic drying of [^{18}F]fluoride at 120 °C for 9 min; labelling of the precursor in MeCN at 100 °C for 6 min; dilution of the crude product with water; tC18 cartridge based purification by use of 20 mL 40% (v/v) Ethanol and 11.5 mL 35% (v/v) Ethanol; elution of the product with 3.5 mL 55% (v/v) Ethanol; formulation with phosphate buffer. RCY 43 ± 9% (n = 10) non d. c., synthesis time 43 min, RCP ≥ 97%.

2.2. Animals

The protocol was based on the approval by the Government of Upper Bavaria (permit number: 55.2-1-54-2532-173-11). All procedures were performed in compliance with the Directive 2010/63/EU of the European Parliament and the Council of 22 September 2010. Twenty-eight adult (200–224 g), female Sprague Dawley rats (Harlan Laboratories, Udine, Italy) were maintained under controlled environmental conditions (22–24 °C; 45–65% humidity) with a constant light/dark cycle of 12 h. Food and water were available ad libitum. Following arrival in our animals facilities, rats were allowed to acclimatize for at least one week. All efforts were made to minimize animal suffering and the number of rats used.

2.3. Electrode implantation

Following anesthesia with chloral hydrate (360 mg/kg, i.p.), bipolar teflon-isolated stainless steel electrodes were stereotactically implanted into the right anterior basolateral nucleus of the amygdala [BLA; AP: − 2.2 mm, LAT: + 4.7 mm, DV: − 8.5 mm; derived from the atlas of Paxinos and Watson (1998)]. Anesthetized rats were placed on a heating pad to maintain a stable body temperature. Meloxicam (Metacam®, Boehringer-Ingelheim, Ingelheim, Germany) (1 mg/kg) was administered subcutaneously (s.c.) 30 min prior to and 24 h post-electrode implantation. Bupivacaine (Bupivacain 0.5%, Jenapharm, Jena, Germany) was applied before exposure of the skull surface to provide additional local anesthesia. In addition, the animals received systemic administration of the antibiotic marbofloxacin (Marbocyl FD 1%, Vétoquinol, Ravensburg, Germany; 1 mg/kg, s.c., twice daily; starting one day before surgery until day 7 post-surgery). Following electrode implantation, rats were allowed to recover for six weeks. Rats were housed individually with daily inspection.

2.4. Electrical induction of a self-sustained status epilepticus

For induction of a self-sustained status epilepticus (SE), 18 rats were electrically stimulated via the BLA electrode by attaching the implanted electrodes to an Accupulser A310C stimulator, which was connected to a Stimulus Isolator A 365 (World Precision Instruments, Berlin, Germany). Stimulation trains (100 ms) consisted of 1 ms alternating positive and negative square-wave pulses (700 μA; duration 25 min; frequency of 2 Hz with an intratrain pulse frequency of 50 Hz). Following stimulation, rats were continuously monitored to detect

behavioral seizure activity. The electroencephalogram (EEG) was recorded via the implanted electrode in all rats before, during and following induction of SE. Epileptic activity was graded according to the Racine (1972): stage 1, eye blinking, and/or facial automatisms such as chewing; stage 2, head nodding and/or more severe facial clonus; stage 3, myoclonic unilateral forelimb clonus; stage 4, bilateral clonic convulsions in the forelimbs with rearing; and stage 5, generalized clonic convulsions associated with rearing and falling. Based on this grading system, SE was scored as type 1 (partial SE consisting of non-convulsive seizure activity and stereotypies), type 2 (partial SE with occasional episodes of generalized seizures) and type 3 (generalized convulsive SE with generalized seizure activity) (Brandt et al., 2003). When animals had experienced SE for 4 h (including the 25 min of SSSE induction), seizure activity was terminated by intraperitoneal injection of diazepam (20 mg/kg, i.p.; Diazepam-Ratiopharm, Ratiopharm, Ulm, Germany). Only rats exhibiting a SE with generalized seizure activity (type 2 or 3; n = 15) were included in subsequent experiments. A group of electrode-implanted controls (n = 8) was not electrically stimulated but handled in parallel including diazepam injection.

2.5. Detection of spontaneous seizures by continuous video/EEG recording

Detection of seizure activity was based on continuous video/EEG-monitoring with the use of infrared light sensitive cameras, a multiple-channel PCI anolog-digital converter (ABUS Security-Tech, Affing, Germany), 1-channel bioamplifiers (BioAmps, AD Instruments, Hastings, East Sussex, United Kingdom), and analog-digital converters (PowerLab/800s, AD Instruments, Hastings, East Sussex, United Kingdom). Video- and EEG-recordings were analyzed using the Digi-Protect Searcher 6.275 beta (ABUS Security-Tech, Affing, Germany) and the Chart5 for windows software (AD Instruments, Hastings, East Sussex, United Kingdom). Two and four weeks following SE induction, continuous video/EEG monitoring was performed during two days prior to PET scanning. Eight to nine weeks following SE induction spontaneous seizure activity was assessed by continuous video/EEG monitoring during two weeks prior to PET scanning. The total number of generalized tonic-clonic motor seizures was recorded including information about the seizure stage (4 or 5). Electrode-implanted control animals were also transiently placed in the monitoring cages and handled in parallel. In addition, seizures observed by video- and EEG-recordings, seizures observed during handling or by direct observation of the animals in their home cages were noted during the entire study.

2.6. Experimental design: longitudinal study

PET imaging was performed two weeks (scan 1), four weeks (scan 2) and ten weeks (scan 3) following SE induction. Fig. 1 shows the timeline of the experiments. Please note that due to issues related to lost electrode assemblies, suspected encephalitis, problems with tracer synthesis, or completed scans but paravenous injections, we were not able to realize a longitudinal follow up for all animals.

Table 1
Injected radioactivity (MBq).

	Electrode-implanted control rats	SE rats
Scan 1	42.2 ± 2.1	44.9 ± 0.7
Scan 2	46.5 ± 1.9	43.9 ± 2.1
Scan 3	47.1 ± 1.1	44.9 ± 1.5

PET data from the following number of animals were analyzed: electrode-implanted control rats n = 5 for all time points and rats with SE n = 6 for the first two time points and n = 9 for the last time point. Supporting Information Table 1 shows the progress of each animal throughout the study. Fig. 2 illustrates the number of animals, in which we managed to complete the analysis of subsequent scanning data.

2.7. Small animal PET experiments

Prior to scanning, rats were anesthetized with 2% isoflurane in 2.0 L/min O_2. Anesthesia was maintained using 1.5–2.0% isoflurane in O_2 at 1 L/min. A cannula was inserted into the tail vein for the injection of the radioligand. After the cannulation, pairs of animals were positioned head to head into the Siemens Inveon P120 PET scanner (Siemens Medical Solutions, Munich, Germany). A bolus injection of [^{18}F]GE-180 (~50 MBq) with a volume of 500 µL saline was administered or given via the cannula of the tail vein at the start of the PET scan. The injection was followed by a saline flush. An emission scan of 60 min was performed for all animals, followed by a transmission scan of 15 min using a rotating ^{57}Co point source. The average injected radioactivity ranged between 42.2 and 47.1 MBq (Table 1). Data were acquired in list mode and reconstructed into 25 timeframes (6 × 20 s, 6 × 30 s, 5 × 60 s, 2 × 150 s, 3 × 300 s, 3 × 600 s). For all PET recordings, reconstruction was performed with 4 OSEM3D and 32 MAP3D iterations, a zoom factor of 1.0, scatter-, attenuation-, and decay-corrected, leading to a final voxel dimension of 0.78 × 0.78 × 0.8 mm. Dynamic datasets were co-registered to a cryosection atlas of the rat brain (Pedersen et al., 2007) by a manual rigid-body transformation after blinding the rat identity to the reader using the PMOD fusion tool (V3.5, PMOD Technologies Ltd.). An extended blood-pool phase 0–30 min was used for this processing. With a second step, a reader-independent fine co-registration to a tracer-specific template was performed. A 0–30 min template was generated by averaging all time point specific PET scans. In the next step the initial manual PET-to-MRI atlas fusion images were normalized by non-

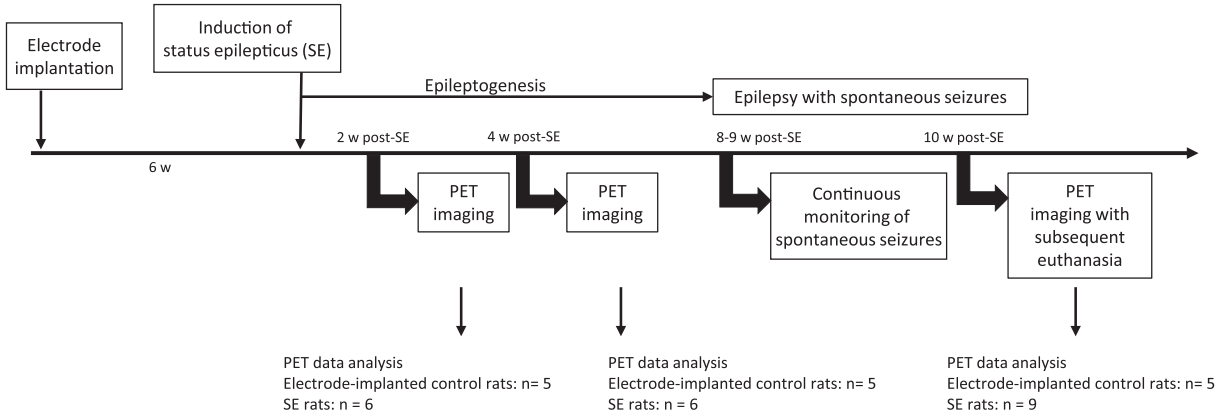

Fig. 1. Study design. Timeline of the experiments.

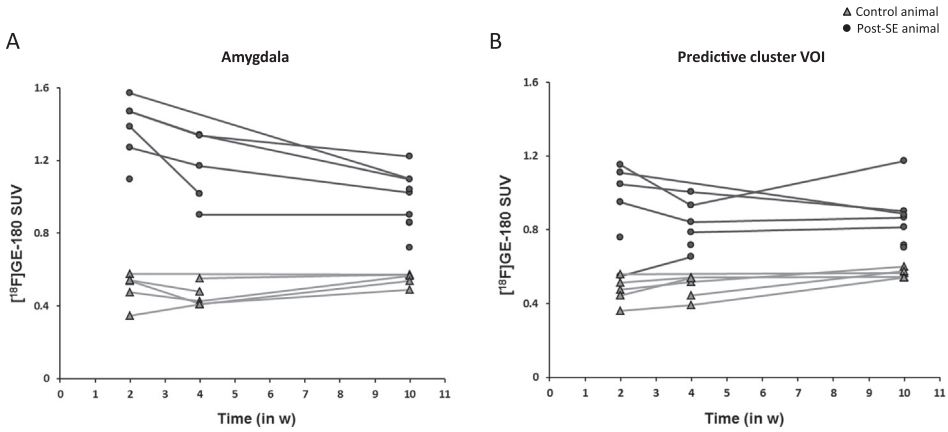

Fig. 2. Longitudinal intra-individual follow-up. Longitudinal intra-individual follow-up for all animals included in at least one of the [^{18}F]GE-180 PET scans. [^{18}F]GE-180 SUVs $_{(30–60\ min)}$ of the amygdala are given in (A), whereas (B) shows values of the predictive cluster VOI.

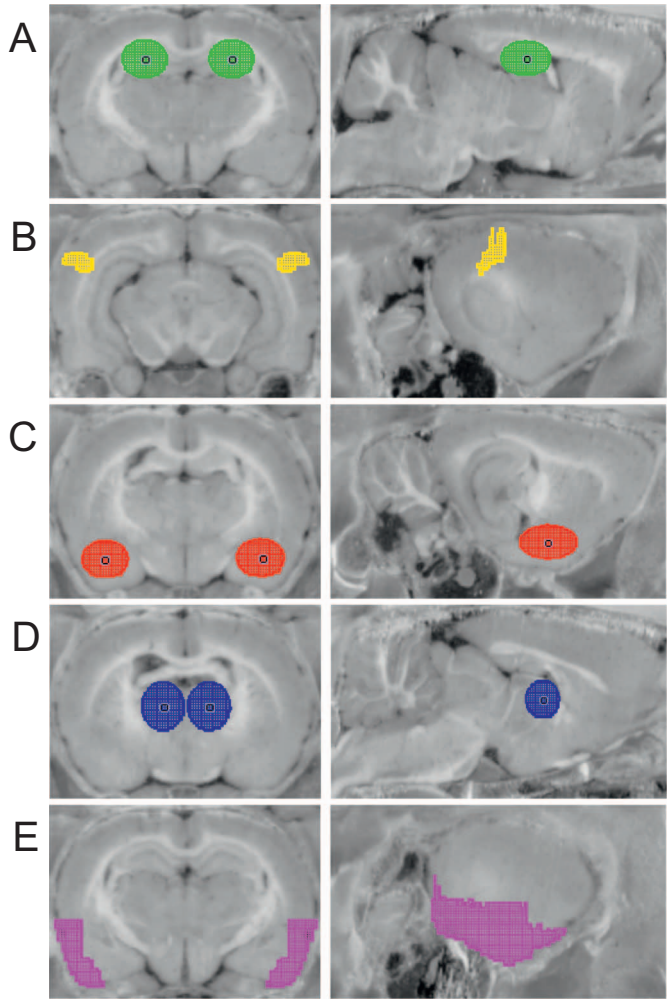

Fig. 3. Analyzed brain regions. Definitions of target regions comprising hippocampus (green, A), parietal cortex (yellow, B), amygdala (red, C), thalamus (blue, D) and entorhinal cortex (violet, E) in the cryosection atlas of the rat brain in coronal and sagittal slices. (For interpretation of the references to color in this figure legend, the reader is referred to the web version of this article.)

linear brain normalization to the tracer-specific template by PMOD brain normalization tool (equal modality; smoothing by 0.8 mm; non-linear warping; 16 iterations; frequency cutoff 3; regularization 1.0; no thresholding) analogous to a previous in-house small animal amyloid-PET study (Overhoff et al., 2016). The concatenation of both transformations was then applied to PET in the native space, so as to obtain optimal resampling with a minimum of interpolation. After dynamic PET analysis the late 30–60 min time frame emerged suitable due to a quantitatively stable ratio TAC for further image and statistical analysis. Thus, $SUV_{30–60}$ data were extracted ($SUV_{30–60}$). 3D bilateral target regions (volumes-of-interest, VOIs) comprising 20 mm^3 for the hippocampus, 15 mm^3 for the parietal cortex, 22 mm^3 for the amygdala, 19 mm^3 for the thalamus and 114 mm^3 for the entorhinal cortex were defined in the cryosection atlas of the rat brain (Pedersen et al., 2007) in coronal, sagittal, and axial sections (Fig. 3). Standardized uptake values (SUV) of all VOIs were calculated by scaling and correcting for the actual intravenously injected dose and multiplying the body weight for [^{18}F]GE-180. Immediately after the end of the third PET scan (ten weeks after SE induction), rats were sacrificed by pentobarbital injection (500 mg/kg i.p.; narcoren®, Merial GmbH, Hallbergmoos, Germany).

2.8. Statistics

Statistical analyses were performed using GraphPad Prism (v 5.0) statistical software. Normality of PET data distribution was assessed by the Kolmogorov-Smirnov test. Parametric data were analyzed by the unpaired *t*-test. Spearman's test was used to test for a possible linear relationship between [^{18}F]GE-180 SUV data and seizure frequency. Data are expressed as means ± SEM. All statistical tests were performed two-sided. Data were considered to be statistically significant when $p < 0.05$.

Voxel-wise comparisons between electrode-implanted control and SE rats were performed by statistical parametric mapping (SPM) using SPM5 routines (Wellcome Department of Cognitive Neurology, London, UK) implemented in MATLAB (version 7.1) (Rominger et al., 2013) for each time point ($SUV_{30–60}$ images). Furthermore, voxel-wise rank based correlation for identification of predictive voxels was performed using $SUV_{30–60}$ images with seizure frequency as a covariate. This analysis was performed with SPM using a multiple regression model. Electrode-implanted control and SE rats were included in this analysis with an additional group covariate to avoid a systematic bias. Single voxels were considered to be statistically significant when they reached an uncorrected p-value < 0.05.

The asymmetry of the [^{18}F]GE-180 SUV at the 30–60 min time frame was quantified by calculating a lateralization index (Lx) as follows: $Lx = (SUV_{30–60}\ \text{left} - SUV_{30–60}\ \text{right}) / (SUV_{30–60}\ \text{left} + SUV_{30–60}\ \text{right})$. The Lx provides a value between −1 and +1 (negative values reflect a right-ward laterality and positive values a left-ward laterality) (Vernaleken et al., 2007).

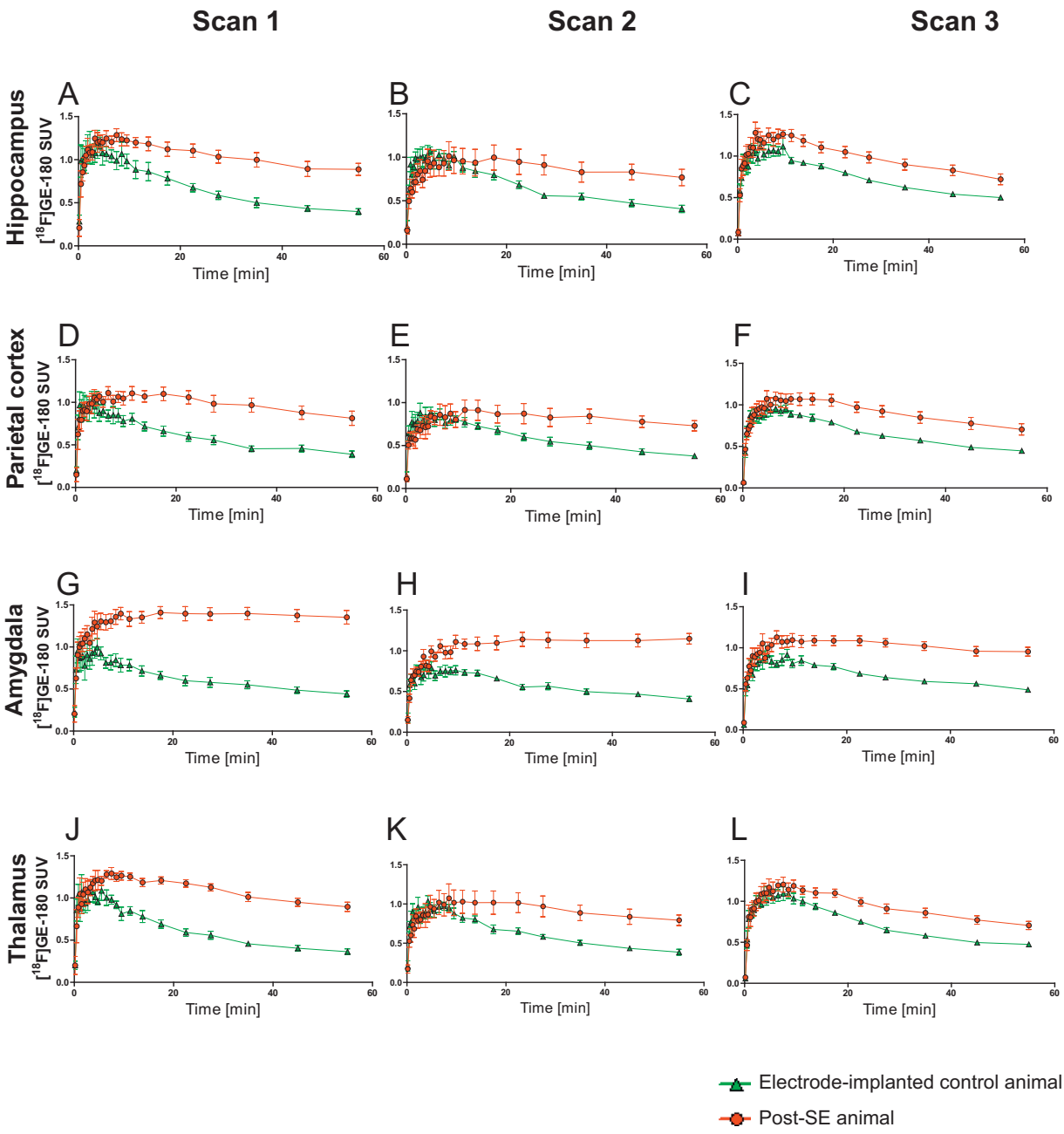

Fig. 4. Time activity curves. Time activity curves of injected [^{18}F]GE-180 for electrode-implanted control animals (n = 5) and post-SE animals (two and four weeks post-SE: n = 6; ten weeks post-SE: n = 9) in the hippocampus (A–C), parietal cortex (D–F), amygdala (G–I), and thalamus (J–L). Radioactivity profile is expressed as SUV and shown for the two time points during the latency phase of epileptogenesis (two weeks post-SE: A, D, G and J; four weeks post-SE: B, E, H and K) and in the early phase following onset of epilepsy with recurrent seizures (ten weeks post-SE: C, F, I and L). The curves indicate that the differences between electrode-implanted control and post-SE groups are most pronounced two weeks following SE in almost all brain regions, and diminish over time. Data shown are mean ± SEM.

3. Results

3.1. Brain uptake of [^{18}F]GE-180 during epileptogenesis

The uptake of [^{18}F]GE-180 to different brain regions of interest known to be involved in generation and spread of seizure activity has been plotted over time to illustrate the influx and stabilization phases (Fig. 4 and Supporting Information Fig. S1). The curves indicate that the differences between electrode-implanted control and SE groups are most pronounced two weeks following SE in almost all brain regions. The impact of the SE is still obvious two weeks later, but further diminishes over time following onset of epilepsy with spontaneous recurrent seizures.

In electrode-implanted control rats, a peak SUV ranging between 0.8 and 1.2 was reached between 2 and 10 min following injection in all brain regions. Washout in electrode-implanted control rats was slow for all regions as already known for this tracer (Brendel et al., 2016). Post-SE animals differed from electrode-implanted control animals and exhibited slowly increasing time-activity curves following the perfusion phase in regions with high TSPO activity like the amygdala (time to peak > 60 min). Other regions indicated a prolonged washout when compared to electrode-implanted control animals. Time activity curves for different brain regions suggest a stabilized binding of [^{18}F]GE-180 after 20–25 min following administration in electrode-implanted control and post-SE animals (Fig. 4). Thus, we have focused the subsequent statistical analysis of SUV data on the late 30–60 min time frame based

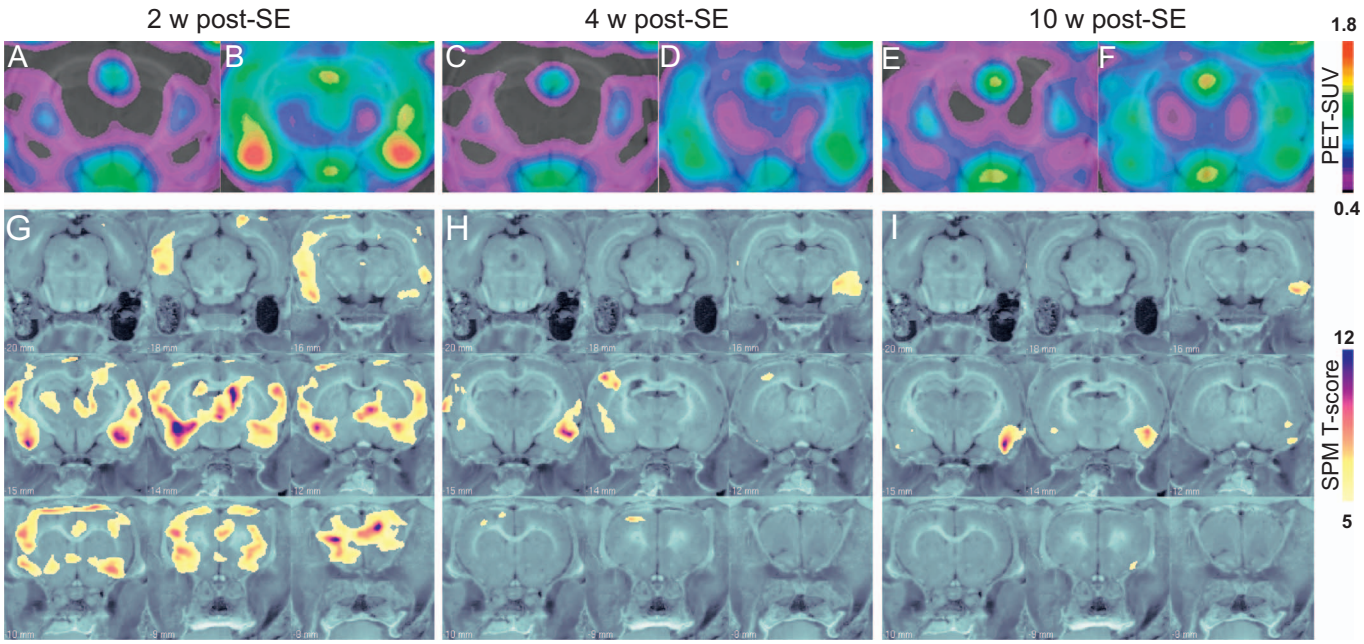

Fig. 5. Coronal views of PET scans. In (A–F), representative coronal views of PET scans demonstrating the distribution of [^{18}F]GE-180 in electrode-implanted control animals (A, C, E) and post-SE animals (B, D, F) are shown for the two time points during the latency phase of epileptogenesis (two weeks post-SE: A and B; four weeks post-SE: C and D) and the early phase following onset of epilepsy with recurrent seizures (ten weeks post-SE: E and F). Coronar depicted voxel-wise SPM analyses are given in (G–I). Whereas the differences to control are widely distributed during the first scan, the brain regions exhibiting pronounced differences seem to be more restricted during scan 2 and 3. Coronal mean SUV maps (A–F) and coronal mean SUV ratio maps (G–I) were projected on the cryosection atlas of the rat brain (gray scale).

on evidence for suitability of late acquisition frames from a recent investigation in Alzheimer disease models using the same radioligand (Brendel et al., 2016).

The importance of neuroinflammation in the majority of brain regions early in epileptogenesis can also be appreciated in the coronal mean SUV maps (Fig. 5A–F) and the coronal depicted voxel-wise SPM analysis (Fig. 5G–I). Differences to control proved to be evident in various brain regions during earlier phases of epileptogenesis. In contrast, brain regions exhibiting pronounced differences seem to be more restricted at the later time point during epileptogenesis and in the chronic phase. Two weeks following SE the [^{18}F]GE-180 $SUV_{30–60}$ proved to be significantly enhanced in the hippocampus, parietal cortex, amygdala, and thalamus (Table 2 and Fig. 6; electrode-implanted control animals n = 5; post-SE animals two and four weeks post-SE: n = 6, ten weeks post-SE: n = 9). The difference to electrode-implanted control animals was most pronounced in the amygdala. In the entorhinal cortex brain uptake in post-SE rats also exceeded that in electrode-implanted control animals (Supporting Information Fig. S2).

With further progression of the latency phase, i.e. four weeks following SE, enhanced levels of [^{18}F]GE-180 brain uptake persisted in all analyzed brain regions (hippocampus, parietal cortex, amygdala, thalamus and entorhinal cortex). However, the difference to electrode-implanted controls proved to be less pronounced in the hippocampus, parietal cortex, amygdala, and thalamus. With regard to the entorhinal cortex, the increase remained in the same range. The difference to electrode-implanted control animals was most pronounced in the amygdala.

During the chronic phase, i.e. ten weeks following SE enhanced levels of [^{18}F]GE-180 brain uptake were maintained in all analyzed brain regions. In the entorhinal cortex, brain uptake in post-SE rats exceeded that in electrode-implanted control animals to a smaller dimension as compared to the other brain regions. The difference to electrode-implanted control animals was again most prominent in the amygdala.

Table 2
Brain uptake of [^{18}F]GE-180.

	Electrode-implanted control rats	SE rats
Two weeks post-SE		
Hippocampus	0.42 ± 0.04	0.96 ± 0.09[a]
Parietal cortex	0.43 ± 0.04	0.89 ± 0.08[a]
Amygdala	0.50 ± 0.04	1.35 ± 0.08[a]
Thalamus	0.40 ± 0.03	0.95 ± 0.05[a]
Entorhinal cortex	0.57 ± 0.04	0.97 ± 0.03[a]
Four weeks post-SE		
Hippocampus	0.45 ± 0.04	0.83 ± 0.10[a]
Parietal cortex	0.44 ± 0.03	0.78 ± 0.07[a]
Amygdala	0.46 ± 0.03	1.13 ± 0.08[a]
Thalamus	0.43 ± 0.03	0.83 ± 0.08[a]
Entorhinal cortex	0.53 ± 0.04	0.89 ± 0.05[a]
Ten weeks post-SE		
Hippocampus	0.52 ± 0.01	0.81 ± 0.06[a]
Parietal cortex	0.50 ± 0.02	0.78 ± 0.07[a]
Amygdala	0.55 ± 0.02	0.98 ± 0.05[a]
Thalamus	0.51 ± 0.01	0.77 ± 0.05[a]
Entorhinal cortex	0.60 ± 0.02	0.83 ± 0.03[a]

[a] Significant to electrode-implanted control rats.

3.2. Asymmetry of [^{18}F]GE-180 uptake during epileptogenesis

As the coronal mean SUV ratio maps indicated an asymmetry of [^{18}F]GE-180 uptake, which seemed to be most pronounced four weeks and ten weeks following SE, we checked whether the two hemispheres differed with regard to the [^{18}F]GE-180 SUV at the 30–60 min time frame. When several regions of the right and the left hemisphere were analyzed separately, Lx calculation revealed a right-side laterality (mean Lx = 0.10 ± 0.03) in the thalamus of electrode-implanted control animals in the early phase and a left-side laterality (mean Lx = 0.06 ± 0.03) in the thalamus of electrode-implanted control animals during the chronic phase. Post-SE animals did not show any significant laterality, neither at the two time points during the latency phase of epileptogenesis nor in the early phase following onset of epilepsy with recurrent seizures. As electrodes were implanted into the right anterior basolateral nucleus of the amygdala, we also checked for

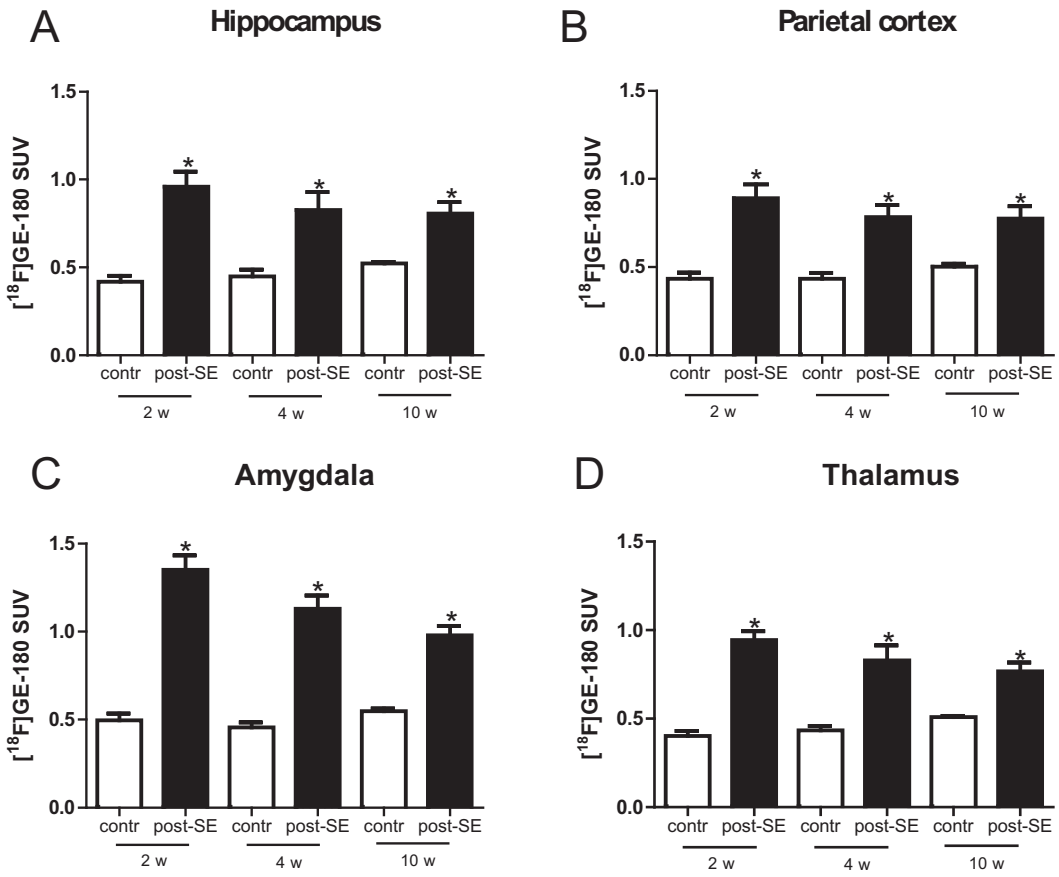

Fig. 6. [^{18}F]GE-180 SUV brain uptake. [^{18}F]GE-180 $SUV_{30–60}$ in the hippocampus (A), parietal cortex (B), amygdala (C) and thalamus (D) of electrode-implanted control animals (n = 5) and post-SE animals (two and four weeks post-SE: n = 6; ten weeks post-SE: n = 9). With further progression of the latency phase enhanced levels of [^{18}F]GE-180 brain uptake persisted in all analyzed brain regions. Data shown are mean ± S.E.M. Significant differences are indicated by asterisks ($p < 0.05$; unpaired *t*-test).

an asymmetry of [^{18}F]GE-180 uptake in the amygdala. Analysis of [^{18}F]GE-180 uptake confirmed that data are in the same range lacking a significant difference between left and right amygdala (Supporting Information Fig. S3).

3.3. Correlation of [^{18}F]GE-180 uptake during the latency period with seizure development

The main question is whether [^{18}F]GE-180 uptake data have predictive value for epileptogenesis. Thus, we have assessed the correlation between SUV data from the latency phase and the development of spontaneous recurrent seizures.

In addition to seizures captured by video- and EEG-recordings, seizures observed during handling or by direct observation of the animals in their home cages were noted during the entire study. During the 2-week continuous video/EEG monitoring phase, spontaneous seizures could be detected in nine out of ten post-SE rats. The number of seizures during the monitoring phase ranged from 0 to 175 with a mean of 21.4 ± 17.2 seizures. EEG- and video-recordings were visually reviewed to detect generalized tonic-clonic motor seizures and the associated characteristic electrographic seizure patterns. The mean additive seizure duration during the 2-week monitoring amounted to 954 ± 700 s. One animal stood out with a relatively high seizure frequency of 175 seizures. The maximum number of seizures per day in this animal reached 25, thus, confirming the occurrence of seizure clusters.

Based on voxel-wise analysis, we tested different brain regions for a correlation between the PET signal and seizure frequency. A correlation was confirmed for the amygdala. Additionally, we identified a predictive cluster VOI comprising parts of different brain regions, including. The hippocampus, parietal cortex, thalamus, somatosensory cortex, and with a minor contribution the amygdala (Fig. 7, Table 3). This cluster VOI comprising a volume of 168 mm^3 also exhibited a positive correlation with seizure frequency. Two weeks following SE, SUV data for the amygdala and the cluster of brain areas correlated positively with the number of seizures recorded during the 2-week monitoring phase (amygdala: r = 0.89. p = 0.00; predictive cluster VOI: r = 0.93, p = 0.00). Interestingly, brain areas with predictive value were not restricted to the ipsilateral hemisphere with the stimulation electrode but were also evident in the contralateral hemisphere (Fig. 7). More detailed analyses revealed that the hippocampus contributes the largest portion to the predictive cluster followed by the parietal cortex and the thalamus (Table 3). Analysis of data from subsequent time points did not reveal a respective positive correlation for these brain regions.

Longitudinal intra-individual follow-up for all animals with a history of an epileptogenic SE demonstrated that [^{18}F]GE-180 SUVs (30–60 min) reached higher levels at all time points in comparison with electrode-implanted control rats (Fig. 2; electrode-implanted control animals n = 5; post-SE animals two and four weeks post-SE: n = 6, ten weeks post-SE: n = 9). Intra-individual follow-up is illustrated for the amygdala and the predictive cluster VOI.

4. Discussion

Here, we provide first experimental evidence that molecular imaging with a high affinity TSPO radioligand such as [^{18}F]GE-180 can predict the development of epilepsy following an epileptogenic brain insult.

In a previous study, we have used the traditional radiotracer (*R*)-[^{11}C]PK11195 to compare rats with drug-responsive and drug-sensitive

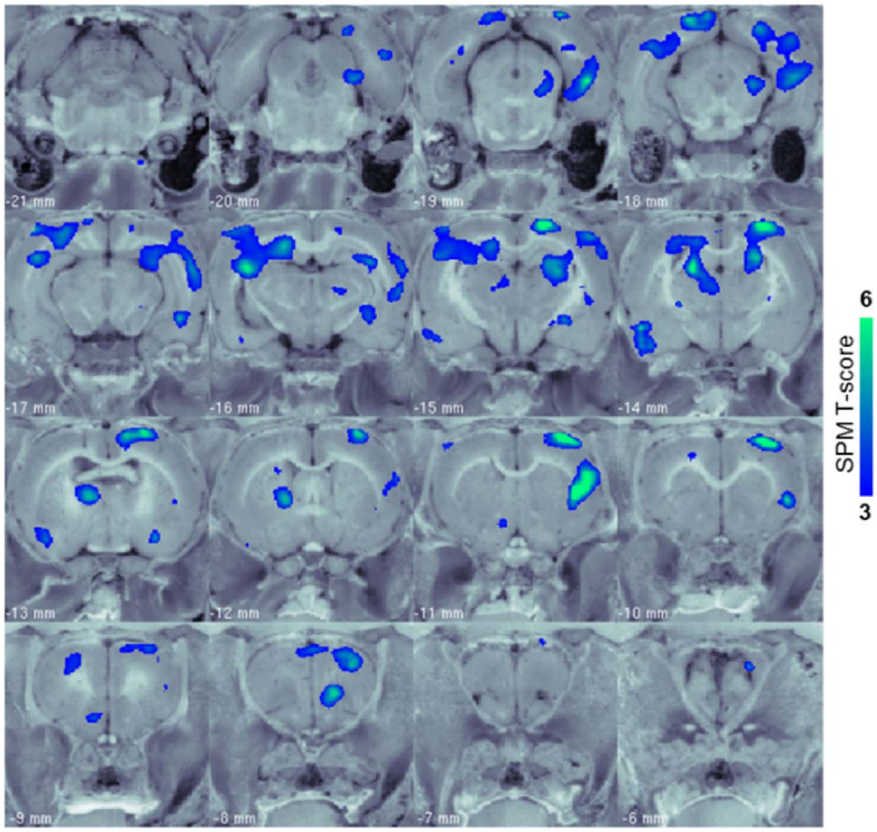

Fig. 7. Coronal map of the predictive cluster VOI. A coronal map of the predictive cluster VOI is shown. The predictive cluster VOI was identified based on correlation analysis considering animals from both groups and comprised parts of different brain regions, e.g. the hippocampus, parietal cortex, thalamus and somatosensory cortex (volume of the predictive cluster VOI: 168 mm^3). The coronal map of the predictive cluster VOI was projected on the cryosection atlas of the rat brain (gray scale).

Table 3
Contribution of different brain regions to the predictive cluster VOI.

VOI	Predictive portion (%)	Predictive volume (mm^3)
Hippocampus	52.0	10.3
Parietal Cortex	36.8	5.5
Thalamus	28.9	5.6
Somatosensory Cortex	19.5	27.2
Visual Cortex	19.5	13.6
Somatomotor Cortex	16.8	15.0
Amygdala	14.9	3.4
Auditory Cortex	12.7	6.6
Entorhinal Cortex	5.2	5.9

spontaneous seizures in the chronic phase of a post-SE model (Bogdanovic et al., 2014). As mentioned above, differences were only evident when comparing non-responders vs. responders or vs. control animals, but not between responders and control rats. Thus, the study suggested that (*R*)-[^{11}C]PK11195 PET is not sensitive enough to assess inflammatory processes associated with epilepsy per se. The present findings confirmed the higher affinity of the novel TSPO radioligand [^{18}F]GE-180, which thus proved to be suitable to detect epileptogenesis- and epilepsy-associated alterations in all animals. These findings are in line with Wadsworth et al. (2012) reporting superiority of [^{18}F]GE-180 with increased brain uptake, affinity, and specificity.

The temporal pattern of [^{18}F]GE-180 SUV during the course of epileptogenesis proved to be characterized by a strong enhancement of uptake in the early phase following the epileptogenic insult, i.e. two weeks following SE. This early increase was followed by a continued decline in the extent and spatial distribution of tracer uptake during the latency phase towards the chronic phase with epilepsy manifestation (four and ten weeks following SE).

An earlier study with analysis of different time points in separate groups of animals described a peak in TSPO expression two weeks following a kainic-acid induced SE (Amhaoul et al., 2015). This study already included a pilot µPET longitudinal analysis using the TSPO tracer [^{18}F]PBR111 in a small group of two (three time points) and four (two time points) animals demonstrating the feasibility of longitudinal PET studies in post-SE models (Amhaoul et al., 2015). However, the lack of seizure monitoring in this subgroup did not allow conclusions about the predictive value of the imaging approach. Further studies with longitudinal analyses have also not included seizure monitoring (Brackhan et al., 2016; Yankam Njiwa et al., 2016). One of these studies has characterized the time course pattern of [^{11}C]PK11195 uptake and binding potential in detail in the pilocarpine-induced post-SE model in rats (Brackhan et al., 2016). The authors reported a maximum regional signal one to two weeks following SE with increases beginning 2–5 days and persisting at least three weeks following SE (Brackhan et al., 2016). Yankam Njiwa et al. (2016) also described an early increase in TSPO binding using [^{11}C]-(*R*)-PK11195 PET six days following a pilocarpine-triggered SE. At a later time point (35 d post-SE) only some animals still exhibited increased levels of tracer binding (Yankam Njiwa et al., 2016). Taken together with our present findings available data suggest a comparable temporal pattern of TSPO radioligand binding in different post-SE models. A more rapid decline suggested by some of the studies might be related to differences between the models as well as tracer characteristics.

The spatial patterns revealed an increase in [^{18}F]GE-180 SUV in different brain regions, which are known to be involved in seizure generation and spread including the hippocampus, parietal cortex, amygdala, thalamus, and entorhinal cortex. Previous studies assessing protein expression of markers linked with inflammatory signaling and microglia activation have demonstrated respective molecular alterations in these brain regions (Borges et al., 2008; Noe et al., 2013;

Vezzani, 2014; Walker et al., 2016).

Similar spatial alterations have been reported for TSPO binding in previous investigations. In the kainic-acid post-SE model enhanced TSPO focal binding proved to be evident in hippocampal subregions, the amygdala, piriform cortex, and entorhinal cortex (Amhaoul et al., 2015). Other groups described increases in uptake and binding of radiolabeled PK11195 in the pilocarpine model in different brain regions including the hippocampus, thalamus, amygdala, and temporal cortex (Brackhan et al., 2016; Yankam Njiwa et al., 2016). Considered cumulatively, the series of experimental PET studies confirms that available TSPO radioligands allow monitoring of inflammatory processes and microglia activation in affected brain regions during the course of epileptogenesis. In this context, we would like to point out that it would be of interest to study TSPO expression in post-mortem tissue analyzing its abundance in microglia vs. astrocytes. We unfortunately failed to establish a robust immunohistochemistry TSPO staining.

Most importantly, our data provide first support that TSPO imaging can render a basis for prediction of epileptogenesis. Our analysis revealed a correlation between [^{18}F]GE-180 SUV in the amygdala and in a cluster of brain regions comprising the hippocampus, parietal cortex, thalamus, and somatosensory cortex, with subsequent development of spontaneous recurrent seizures. All of these regions are known to be affected on a cellular and network level during epileptogenesis (Nairismagi et al., 2004; Scholl et al., 2013). The fact that the hippocampus was standing out as a main region of the predictive cluster VOI is not surprising considering that its insult-induced dysfunction as a gate of activity processing is considered as one contributor to epileptogenesis (Sierra et al., 2015). In this context it is of interest that inflammatory mediators can enhance excitability of neurons based on an impact on neurotransmitter receptor functional states (Biagini et al., 2012; Iori et al., 2016).

Our findings suggest [^{18}F]GE-180 SUV as a putative biomarker of epilepsy development following epileptogenic brain insults. Respective biomarkers are urgently needed for patient stratification following insults and for the follow-up of the efficacy of clinical intervention trials assessing antiepileptogenic strategies (Schmidt, 2012; Pitkanen et al., 2013; Trinka and Brigo, 2014; Pitkanen et al., 2016). In experimental studies respective biomarkers might serve as valuable tools decreasing the workload associated with the testing of preventive approaches otherwise requiring week-long seizure monitoring (Dedeurwaerdere et al., 2014). Of course the validity as a biomarker candidate requires further assessment. Considering that only one animal in our study did not develop epilepsy further validation will be necessary in a model with subgroups of rats with or without epilepsy development following a brain insult. In addition, it would be interesting to assess TSPO PET development in animals with a non-generalized SE. Moreover, it will be of particular relevance to test the validity in models with different types of insults including traumatic brain injury or brain ischemia.

Interestingly, the predictive value of data from the amygdala and the cluster VOI proved to be bilateral despite the electrical induction of the initial SE via a depth electrode in the right amygdala. The bilateral nature of the SUV alterations is however consistent with previous findings describing bilateral molecular and cellular alterations in the electrical post-SE model used in this study (Brandt et al., 2003; Brandt et al., 2007).

The correlation between [^{18}F]GE-180 SUV and seizure development also provides further confirmation for a functional relevance of the degree of inflammation for the long-term outcome following an epileptogenic brain insult. During the last two decades experimental and clinical studies provided strong cumulative evidence for a key role of excessive inflammatory signaling in the development of a hyperexcitable epileptic network (Devinsky et al., 2013; Vezzani et al., 2013). Convincing support for a significant contribution to epileptogenesis came from a series of studies with genetic or pharmacological targeting strategies resulting in antiepileptogenic effects in rodent models (Maroso et al., 2011; Ravizza et al., 2011; Noe et al., 2013; Vitaliti et al., 2014; Vezzani, 2015).

Excessive inflammation has already been described in surgical specimen and post-mortem tissue from human patients with temporal lobe epilepsy (Aronica and Crino, 2011; Das et al., 2012; Vezzani et al., 2016; Volmering et al., 2016). In this context, an immunohistochemistry analysis confirmed an overexpression of TSPO in surgical tissue (Sauvageau et al., 2002). Taking this into account efforts have also been made to assess epilepsy-associated alterations by clinical application of TSPO PET. An increased uptake of a TSPO radioligand has been reported by Hirvonen et al. (2012). A more recent study analyzed the distribution of the TSPO tracer [^{11}C]PBR28 in a cohort of patients with TLE (Gershen et al., 2015). The authors concluded that TSPO is increased ipsi- and contralaterally to seizure foci in patients.

When considering the data presented the limitations of the study need to be taken into account. We would like to point out the given variance of quantitative PET, the difficulties in completing series of subsequent PET scans in a group of epileptic animals and related to this issue the low animal numbers, which might affect the robustness of the prediction analysis. Nonetheless our so far limited but encouraging results emphasize the need of further research regarding the predictive value of TSPO PET for epileptogenesis.

To our knowledge, there are no clinical data yet available assessing a correlation between TSPO imaging data following putative epileptogenic brain insults and the long-term outcome. Based on our present findings, respective studies might be of interest following further experimental validation of the imaging approach. Respective translational research will be of particular relevance also considering that the time course of epileptogenesis with some weeks in the animal model used translates to months and years in patients with differences depending on the patient, the brain insult and its severity. Thus, any clinical validation of a biomarker candidate needs to carefully assess the time windows during which analysis of the marker results in predictive data.

In conclusion, the data provide first evidence that [^{18}F]GE-180 PET brain imaging can serve as a biomarker of epileptogenesis. The identification of brain regions with predictive value might facilitate the development of preventive concepts as well as the early assessment of the interventional success. Future studies are necessary to further confirm the predictivity of the approach.

The authors declare that they do not have any conflict of interest.

Acknowledgements

The authors thank Karin Bormann-Giglmaier, Marion Fisch, Sieglinde Fischlein, Barbara Kohler, Rosel Oos, Regina Rentsch, Maruja L. Rettenbeck and Claudia Siegl for their technical assistance. GE-180 cassettes were received from GE.

Appendix A. Supplementary data

Supplementary data to this article can be found online at http://dx.doi.org/10.1016/j.nicl.2017.04.003.

References

Amhaoul, H., Staelens, S., Dedeurwaerdere, S., 2014. Imaging brain inflammation in epilepsy. Neuroscience 279, 238–252.

Amhaoul, H., Hamaide, J., Bertoglio, D., Reichel, S.N., Verhaeghe, J., Geerts, E., Van Dam, D., De Deyn, P.P., Kumar-Singh, S., Katsifis, A., Van Der Linden, A., Staelens, S., Dedeurwaerdere, S., 2015. Brain inflammation in a chronic epilepsy model: evolving pattern of the translocator protein during epileptogenesis. Neurobiol. Dis. 82, 526–539.

Aronica, E., Crino, P.B., 2011. Inflammation in epilepsy: clinical observations. Epilepsia 52 (Suppl. 3), 26–32.

Biagini, G., Marinelli, C., Panuccio, G., Puia, G., Avoli, M., 2012. Glia-neuron interactions: Neurosteroids and epileptogenesis. In: Noebels, J.L., Avoli, M., Rogawski, M.A., Olsen, R.W., Delgado-Escueta, A.V. (Eds.), Jasper's Basic Mechanisms of the

Epilepsies, (Bethesda (MD)).
Bogdanovic, R.M., Syvanen, S., Michler, C., Russmann, V., Eriksson, J., Windhorst, A.D., Lammertsma, A.A., de Lange, E.C., Voskuyl, R.A., Potschka, H., 2014. (R)-[^{11}C] PK11195 brain uptake as a biomarker of inflammation and antiepileptic drug resistance: evaluation in a rat epilepsy model. Neuropharmacology 85, 104–112.
Borges, K., Gearing, M., Rittling, S., Sorensen, E.S., Kotloski, R., Denhardt, D.T., Dingledine, R., 2008. Characterization of osteopontin expression and function after status epilepticus. Epilepsia 49, 1675–1685.
Brackhan, M., Bascunana, P., Postema, J.M., Ross, T.L., Bengel, F.M., Bankstahl, M., Bankstahl, J.P., 2016. Serial quantitative TSPO-targeted PET reveals peak microglial activation up to 2 weeks after an epileptogenic brain insult. J. Nucl. Med. Off. Publ. Soc. Nucl. Med. 57, 1302–1308.
Brandt, C., Glien, M., Potschka, H., Volk, H., Loscher, W., 2003. Epileptogenesis and neuropathology after different types of status epilepticus induced by prolonged electrical stimulation of the basolateral amygdala in rats. Epilepsy Res. 55, 83–103.
Brandt, C., Glien, M., Gastens, A.M., Fedrowitz, M., Bethmann, K., Volk, H.A., Potschka, H., Loscher, W., 2007. Prophylactic treatment with levetiracetam after status epilepticus: lack of effect on epileptogenesis, neuronal damage, and behavioral alterations in rats. Neuropharmacology 53, 207–221.
Brendel, M., Probst, F., Jaworska, A., Overhoff, F., Korzhova, V., Albert, N.L., Beck, R., Lindner, S., Gildehaus, F.J., Baumann, K., Bartenstein, P., Kleinberger, G., Haass, C., Herms, J., Rominger, A., 2016. Glial activation and glucose metabolism in a transgenic amyloid mouse model: a triple-tracer PET study. J. Nucl. Med. Off. Publ. Soc. Nucl. Med. 57, 954–960.
Ching, A.S., Kuhnast, B., Damont, A., Roeda, D., Tavitian, B., Dolle, F., 2012. Current paradigm of the 18-kDa translocator protein (TSPO) as a molecular target for PET imaging in neuroinflammation and neurodegenerative diseases. Insights Into Imaging 3, 111–119.
Das, A., Wallace, G.C.T., Holmes, C., McDowell, M.L., Smith, J.A., Marshall, J.D., Bonilha, L., Edwards, J.C., Glazier, S.S., Ray, S.K., Banik, N.L., 2012. Hippocampal tissue of patients with refractory temporal lobe epilepsy is associated with astrocyte activation, inflammation, and altered expression of channels and receptors. Neuroscience 220, 237–246.
Dedeurwaerdere, S., Callaghan, P.D., Pham, T., Rahardjo, G.L., Amhaoul, H., Berghofer, P., Quinlivan, M., Mattner, F., Loc'h, C., Katsifis, A., Gregoire, M.C., 2012. PET imaging of brain inflammation during early epileptogenesis in a rat model of temporal lobe epilepsy. EJNMMI Res. 2, 60.
Dedeurwaerdere, S., Shultz, S.R., Federico, P., Engel Jr., J., 2014. Workshop on neurobiology of epilepsy appraisal: new systemic imaging technologies to study the brain in experimental models of epilepsy. Epilepsia 55, 819–828.
Devinsky, O., Vezzani, A., Najjar, S., De Lanerolle, N.C., Rogawski, M.A., 2013. Glia and epilepsy: excitability and inflammation. Trends Neurosci. 36, 174–184.
Gershen, L.D., Zanotti-Fregonara, P., Dustin, I.H., Liow, J.S., Hirvonen, J., Kreisl, W.C., Jenko, K.J., Inati, S.K., Fujita, M., Morse, C.L., Brouwer, C., Hong, J.S., Pike, V.W., Zoghbi, S.S., Innis, R.B., Theodore, W.H., 2015. Neuroinflammation in temporal lobe epilepsy measured using positron emission tomographic imaging of translocator protein. JAMA Neurol. 72, 882–888.
Hirvonen, J., Kreisl, W.C., Fujita, M., Dustin, I., Khan, O., Appel, S., Zhang, Y., Morse, C., Pike, V.W., Innis, R.B., Theodore, W.H., 2012. Increased in vivo expression of an inflammatory marker in temporal lobe epilepsy. J. Nucl. Med. Off. Publ. Soc. Nucl. Med. 53, 234–240.
Iori, V., Frigerio, F., Vezzani, A., 2016. Modulation of neuronal excitability by immune mediators in epilepsy. Curr. Opin. Pharmacol. 26, 118–123.
James, M.L., Belichenko, N.P., Nguyen, T.V., Andrews, L.E., Ding, Z., Liu, H., Bodapati, D., Arksey, N., Shen, B., Cheng, Z., Wyss-Coray, T., Gambhir, S.S., Longo, F.M., Chin, F.T., 2015. PET imaging of translocator protein (18 kDa) in a mouse model of Alzheimer's disease using N-(2,5-dimethoxybenzyl)-2-18F-fluoro-N-(2-phenoxyphenyl)acetamide. J. Nucl. Med. Off. Publ. Soc. Nucl. Med. 56, 311–316.
Maroso, M., Balosso, S., Ravizza, T., Liu, J., Bianchi, M.E., Vezzani, A., 2011. Interleukin-1 type 1 receptor/Toll-like receptor signalling in epilepsy: the importance of IL-1beta and high-mobility group box 1. J. Intern. Med. 270, 319–326.
Nairismagi, J., Grohn, O.H., Kettunen, M.I., Nissinen, J., Kauppinen, R.A., Pitkanen, A., 2004. Progression of brain damage after status epilepticus and its association with epileptogenesis: a quantitative MRI study in a rat model of temporal lobe epilepsy. Epilepsia 45, 1024–1034.
Noe, F.M., Polascheck, N., Frigerio, F., Bankstahl, M., Ravizza, T., Marchini, S., Beltrame, L., Bandero, C.R., Loscher, W., Vezzani, A., 2013. Pharmacological blockade of IL-1beta/IL-1 receptor type 1 axis during epileptogenesis provides neuroprotection in two rat models of temporal lobe epilepsy. Neurobiol. Dis. 59, 183–193.
Overhoff, F., Brendel, M., Jaworska, A., Korzhova, V., Delker, A., Probst, F., Focke, C., Gildehaus, F.J., Carlsen, J., Baumann, K., Haass, C., Bartenstein, P., Herms, J., Rominger, A., 2016. Automated spatial brain normalization and hindbrain white matter reference tissue give improved [(18)F]-Florbetaben PET quantitation in Alzheimer's model mice. Front. Neurosci. 10, 45.
Paxinos, G., Watson, C., 1998. The Rat Brain in Stereotactic Coordinates. Academic Press (Sydney).
Pedersen, K., Simonsen, M., Ostergaard, S.D., Munk, O.L., Rosa-Neto, P., Olsen, A.K., Jensen, S.B., Moller, A., Cumming, P., 2007. Mapping the amphetamine-evoked changes in [^{11}C]raclopride binding in living rat using small animal PET: modulation by MAO-inhibition. NeuroImage 35, 38–46.
Pitkanen, A., Engel Jr., J., 2014. Past and present definitions of epileptogenesis and its biomarkers. Neurotherapeutics 11, 231–241.
Pitkanen, A., Nehlig, A., Brooks-Kayal, A.R., Dudek, F.E., Friedman, D., Galanopoulou, A.S., Jensen, F.E., Kaminski, R.M., Kapur, J., Klitgaard, H., Loscher, W., Mody, I., Schmidt, D., 2013. Issues related to development of antiepileptogenic therapies. Epilepsia 54 (Suppl. 4), 35–43.
Pitkanen, A., Loscher, W., Vezzani, A., Becker, A.J., Simonato, M., Lukasiuk, K., Grohn, O., Bankstahl, J.P., Friedman, A., Aronica, E., Gorter, J.A., Ravizza, T., Sisodiya, S.M., Kokaia, M., Beck, H., 2016. Advances in the development of biomarkers for epilepsy. Lancet Neurol. 15, 843–856.
Politis, M., Lahiri, N., Niccolini, F., Su, P., Wu, K., Giannetti, P., Scahill, R.I., Turkheimer, F.E., Tabrizi, S.J., Piccini, P., 2015. Increased central microglial activation associated with peripheral cytokine levels in premanifest Huntington's disease gene carriers. Neurobiol. Dis. 83, 115–121.
Racine, R.J., 1972. Modification of seizure activity by electrical stimulation. II. Motor seizure. Electroencephalogr. Clin. Neurophysiol. 32, 281–294.
Rao, V.R., Parko, K.L., 2015. Clinical approach to posttraumatic epilepsy. Semin. Neurol. 35, 57–63.
Ravizza, T., Balosso, S., Vezzani, A., 2011. Inflammation and prevention of epileptogenesis. Neurosci. Lett. 497, 223–230.
Rominger, A., Brendel, M., Burgold, S., Keppler, K., Baumann, K., Xiong, G., Mille, E., Gildehaus, F.J., Carlsen, J., Schlichtiger, J., Niedermoser, S., Wangler, B., Cumming, P., Steiner, H., Herms, J., Haass, C., Bartenstein, P., 2013. Longitudinal assessment of cerebral beta-amyloid deposition in mice overexpressing Swedish mutant beta-amyloid precursor protein using 18F-florbetaben PET. J. Nucl. Med. Off. Publ. Soc. Nucl. Med. 54, 1127–1134.
Sauvageau, A., Desjardins, P., Lozeva, V., Rose, C., Hazell, A.S., Bouthillier, A., Butterwort, R.F., 2002. Increased expression of “peripheral-type” benzodiazepine receptors in human temporal lobe epilepsy: implications for PET imaging of hippocampal sclerosis. Metab. Brain Dis. 17, 3–11.
Schmidt, D., 2012. Is antiepileptogenesis a realistic goal in clinical trials? Concerns and new horizons. Epileptic Disord. 14, 105–113.
Scholl, E.A., Dudek, F.E., Ekstrand, J.J., 2013. Neuronal degeneration is observed in multiple regions outside the hippocampus after lithium pilocarpine-induced status epilepticus in the immature rat. Neuroscience 252, 45–59.
Sierra, A., Grohn, O., Pitkanen, A., 2015. Imaging microstructural damage and plasticity in the hippocampus during epileptogenesis. Neuroscience 309, 162–172.
Trinka, E., Brigo, F., 2014. Antiepileptogenesis in humans: disappointing clinical evidence and ways to move forward. Curr. Opin. Neurol. 27, 227–235.
Venneti, S., Lopresti, B.J., Wiley, C.A., 2013. Molecular imaging of microglia/macrophages in the brain. Glia 61, 10–23.
Vernaleken, I., Weibrich, C., Siessmeier, T., Buchholz, H.G., Rosch, F., Heinz, A., Cumming, P., Stoeter, P., Bartenstein, P., Grunder, G., 2007. Asymmetry in dopamine D(2/3) receptors of caudate nucleus is lost with age. NeuroImage 34, 870–878.
Vezzani, A., 2014. Epilepsy and inflammation in the brain: overview and pathophysiology. Epilepsy Curr. 14, 3–7.
Vezzani, A., 2015. Anti-inflammatory drugs in epilepsy: does it impact epileptogenesis? Expert Opin. Drug Saf. 14, 583–592.
Vezzani, A., Friedman, A., 2011. Brain inflammation as a biomarker in epilepsy. Biomark. Med 5, 607–614.
Vezzani, A., Friedman, A., Dingledine, R.J., 2013. The role of inflammation in epileptogenesis. Neuropharmacology 69, 16–24.
Vezzani, A., Lang, B., Aronica, E., 2016. Immunity and inflammation in epilepsy. Cold Spring Harb. Perspect. Med. 6, a022699.
Vitaliti, G., Pavone, P., Mahmood, F., Nunnari, G., Falsaperla, R., 2014. Targeting inflammation as a therapeutic strategy for drug-resistant epilepsies: an update of new immune-modulating approaches. Hum. Vaccines Immunotherapeutics 10, 868–875.
Volmering, E., Niehusmann, P., Peeva, V., Grote, A., Zsurka, G., Altmuller, J., Nurnberg, P., Becker, A.J., Schoch, S., Elger, C.E., Kunz, W.S., 2016. Neuropathological signs of inflammation correlate with mitochondrial DNA deletions in mesial temporal lobe epilepsy. Acta Neuropathol. 132, 277–288.
Wadsworth, H., Jones, P.A., Chau, W.F., Durrant, C., Fouladi, N., Passmore, J., O'Shea, D., Wynn, D., Morisson-Iveson, V., Ewan, A., Thaning, M., Mantzilas, D., Gausemel, I., Khan, I., Black, A., Avory, M., Trigg, W., 2012. [(1)(8)F]GE-180: a novel fluorine-18 labelled PET tracer for imaging translocator protein 18 kDa (TSPO). Bioorg. Med. Chem. Lett. 22, 1308–1313.
Walker, A., Russmann, V., Deeg, C.A., von Toerne, C., Kleinwort, K.J., Szober, C., Rettenbeck, M.L., von Ruden, E.L., Goc, J., Ongerth, T., Boes, K., Salvamoser, J.D., Vezzani, A., Hauck, S.M., Potschka, H., 2016. Proteomic profiling of epileptogenesis in a rat model: focus on inflammation. Brain Behav. Immun. 53, 138–158.
Weiss, G.H., Salazar, A.M., Vance, S.C., Grafman, J.H., Jabbari, B., 1986. Predicting posttraumatic epilepsy in penetrating head injury. Arch. Neurol. 43, 771–773.
Wickstrom, T., Clarke, A., Gausemel, I., Horn, E., Jorgensen, K., Khan, I., Mantzilas, D., Rajanayagam, T., in 't Veld, D.J. & Trigg, W., 2014. The development of an automated and GMP compliant FASTlab synthesis of [(18) F]GE-180; a radiotracer for imaging translocator protein (TSPO). J. Label. Compd. Radiopharm. 57, 42–48.
Yankam Njiwa, J., Costes, N., Bouillot, C., Bouvard, S., Fieux, S., Becker, G., Levigoureux, E., Kocevar, G., Stamile, C., Langlois, J.B., Bolbos, R., Bonnet, C., Bezin, L., Zimmer, L., Hammers, A., 2016. Quantitative longitudinal imaging of activated microglia as a marker of inflammation in the pilocarpine rat model of epilepsy using [^{11}C]-(R)-PK11195 PET and MRI. J. Cereb. Blood Flow Metab.
Zurcher, N.R., Loggia, M.L., Lawson, R., Chonde, D.B., Izquierdo-Garcia, D., Yasek, J.E., Akeju, O., Catana, C., Rosen, B.R., Cudkowicz, M.E., Hooker, J.M., Atassi, N., 2015. Increased in vivo glial activation in patients with amyotrophic lateral sclerosis: assessed with [(11)C]-PBR28. NeuroImage. Clin. 7, 409–414.